Lejie Liu
Department of Mechanical Engineering,
University of Wisconsin-Madison,
1513 University Avenue,
Madison, WI 53706
e-mail: lliu265@wisc.edu

Karthik Yerrapragada
Department of Mechanical Engineering,
University of Wisconsin-Madison,
1513 University Avenue,
Madison, WI 53706
e-mail: yerrapragada@wisc.edu

Corinne R. Henak
Department of Mechanical Engineering;
Department of Orthopedics and Rehabilitation;
Department of Biomedical Engineering,
University of Wisconsin-Madison,
1513 University Avenue,
Madison, WI 53706
e-mail: chenak@wisc.edu

Melih Eriten[1]
Department of Mechanical Engineering,
University of Wisconsin-Madison,
1513 University Avenue,
Madison, WI 53706
e-mail: eriten@wisc.edu

Contact Nonlinearity in Indenter–Foam Dampers

In this paper, the nonlinear response of indenter–foam dampers is characterized. Those dampers consist of indenters pressed on open-cell foams swollen with wetting liquids. Recently, the authors identified the dominant mechanism of damping in those dampers as poro-viscoelastic (PVE) relaxations as in articular cartilage, one of nature's best solutions to vibration attenuation. Those previous works by the authors included dynamic mechanical analyses of the indenter–foam dampers under small vibrations, i.e., linear regime. The current study features the dynamic response of similar dampers under larger strains to investigate the nonlinear regime. In particular, the indenter–foam dampers tested in this paper consist of an open-cell polyurethane foam swollen with castor oil. Harmonic displacements are applied on the swollen and pre-compressed foam using a flat-ended cylindrical indenter. Measured forces and corresponding hysteresis (force–displacement) loops are then analyzed to quantify damping performance (via specific damping capacity) and nonlinearities (via harmonic ratio). The effects of strain and strain rates on the damping capacity and harmonic ratio are investigated experimentally. The dominant source of the nonlinearity is identified as peeling at the indenter–foam interface (and quantified via peeling index). A representative model consisting of a linear viscoelastic foam and rate-dependent adhesive interface (slider element with limiting adhesive strength) explains the observed trends in peeling and thus nonlinear dynamic response. Possible remedies to suppress those nonlinearities in future designs of indenter–foam dampers are also discussed.
[DOI: 10.1115/1.4054054]

Keywords: poro-viscoelasticity, indenter–foam dampers, specific damping capacity, harmonic ratio, peeling index, contact nonlinearity, materials in vibration and acoustics, nonlinear vibration, vibration control

1 Introduction

Energy dissipation as often achieved by dampers in a prescribed frequency range is essential for vibration suppression in engineered systems. Dampers can be categorized as active, semi-active, or passive depending on the existence and complexity of feedback control in the system [1]. Active damping is used when high performance is critical and/or the host system operates under highly transient and uncertain conditions. Active dampers usually comprise sensors, actuators, and controllers that add complexity, weight, power consumption, and cost to a particular system design [2]. Semi-active dampers still have the control mechanism but with the absence of an actuator mechanism that active dampers have [3]. Active and semi-active dampers usually achieve broadband effectiveness, but are accompanied by high cost and complex mechanisms. Passive dampers, in contrast, offer cost-effective vibration suppression via the utilization of dissipative components and materials without feedback control. However, most of the existing passive dampers lack broadband effectiveness and adaptation to operating conditions that require different levels of energy dissipation.

The indenter–foam dampers developed by the authors provide passive damping by poro-viscoelastic relaxations. Before a detailed analysis of those dampers, several recent passive damper designs with similar damping mechanisms are worth mentioning. For instance, McNamara et al. introduce annular tuned liquid dampers (TLD) that can be mounted in slender structures [4]. An equivalent linearized model is developed to accurately predict the energy dissipation per cycle obtained from a practical model. The paper concludes that annular TLD attached to a slender structure provided comparable performance to tuned-mass dampers in the linearized regime for a range of excitation amplitudes [4]. Wong and Wong propose a four-element air damper dynamic vibration absorber using Maxwell and Coulomb elements and show that their design reduced the vibration levels by 19% when compared to traditional three-element dampers, which consisted of two springs and viscous element [5]. Love et al. proposed a pendulum-type mass damper tuned to sloshing to reduce wind-induced structural motion [6]. The sloshing system is used to provide additional restoring forces, and the damper is shown to provide comparable performance to a traditional tuned-mass damper. In that design, the absence of viscous damping component proves cost-effectiveness. Javidialesaadi and Wierschem introduce a three-element vibration-absorber inerter, which has a rotating mass due to the relative translational motion of the two masses [7]. The proposed inerter is shown to deliver better damping performance than the standard tuned-mass-damper-inerter system. Verbaan et al. [8] developed a linear viscoelastic damper to suppress vibrations in spring-mass systems. The proposed damper showed effectiveness at lower frequencies (<1 kHz) when compared to the higher frequencies of a motion stage. Note that the mentioned studies mainly focus on the performance of passive dampers in the linearized regimes.

With the aim of obtaining cost-effective dampers with broadband effectiveness, the authors have developed and tested novel PVE indenter–foam damper designs for the last five years. Indenter–foam dampers consist of indenters that transmit vibration to PVE media, and the vibrations are attenuated via multiple physical mechanisms: viscoelasticity, diffusion, and fluid–solid frictional interactions. Different from other passive dampers, PVE indenter–foam dampers recruit both interfacial and material damping simultaneously and thus resemble articular cartilage at the ends of mammalian long bones. In 2016, the current authors optimized a set of indenter–foam dampers to introduce broadband damping capacity [9]. A PVE foam was sandwiched between two hard materials,

[1]Corresponding author.

Contributed by the Technical Committee on Vibration and Sound of ASME for publication in the Journal of Vibration and Acoustics. Manuscript received November 28, 2021; final manuscript received March 3, 2022; published online March 24, 2022. Assoc. Editor: James Gibert.

and vibrations were transmitted to that layer via multiple indenters of varying contact lengths. Optimizing those contact lengths then enabled a nearly constant loss factor for a broad frequency range (3–3000 Hz), i.e., an effective broadband damper. The authors then utilized the same dampers in fuzzy oscillators and demonstrated tunable vibration absorption around modes of a host structure [10]. Finally, the authors reported the damping capacity of foam-indenter dampers in single- and double-indenter configurations [11]. The dampers included rigid cylindrical indenters pressed on open-cell polyethylene foams swollen with Newtonian fluids. Dynamic mechanical analysis (DMA) of the indenters over a frequency range of 0.5–100 Hz delivered significant damping capacity (phase angles around 40 deg). The experimental observations validated both the narrow and broadband performance of those dampers under small oscillations of the indenters over a frequency range of 0.5–100 Hz. The experimental observations suggest single-indenter configuration delivered narrowband performance and the double-indenter configuration delivered broadband performance of those dampers in a linear regime. Those tests demonstrated that the simple and cost-effective design of indenter–foam dampers delivers damping capacities comparable to other material or viscoelastic dampers [11], yet damping capacity can be tuned for broadband [9] or narrowband [10] applications.

In those earlier works, the small oscillation assumption allowed us to model the indenter–foam system with linearized PVE models that neglect complications such as material and contact nonlinearities. The maximum strains investigated in this study are around 2.5%. For typical open-cell foams, those strains correspond to the linear elastic response. Thus, the focus of this study will be on interfacial nonlinearities. PVE relaxations lead to a reduction in residual compressive stresses, and thus, subsequent vibrations can apply tension in parts of loading cycles with moderate-to-large amplitudes. Adhesion of PVE materials to rigid surfaces is known to increase with the unloading rates [12–16]. Combination of strains and strain rates lead to a build-up of tensile stresses in PVE materials that could eventually overcome adhesive strength and cause peeling at the indenter–foam interface. The peeling effect results in an asymmetric reduction in stiffness and hence contact nonlinearity during a loading cycle. The degree of contact nonlinearity, its dependence on strains and strain rates, and effects on the performance of indenter–foam dampers remain unexplored in the literature. To fill that gap, the contact nonlinearity in indenter–foam dampers is studied experimentally in the current work. The loss of contact at the interface would result in some artificial damping effect in the system through reduced stored energy. A possible remedy is suggested to suppress the nonlinearities for future damper designs to accurately estimate the damping capacities.

The paper is outlined as follows: In Sec. 2, preparation of the indenter–foam damper and the experimental setup for the DMA is described. In Sec. 3, the results, namely the amount of contact peeling, corresponding loss of contact stiffness, and degree of nonlinearity are reported as maps of strains and strain rates. Those maps provide guidelines for linear and nonlinear designs of indenter–foam dampers. Discussions are included as subsections in the results (Sec. 3). Section 4 concludes the paper.

2 Experiments and Methods

2.1 Indenter–Foam Damper Preparation. Open-cell polyurethane foams (New England Foam Co., Hartford, CT) swollen with castor oil (Naissance Ltd., Neath, UK) were used as the PVE material of the dampers [11]. The combination of selected foams and liquid ensured a low Reynolds number (0.04 in this case) so that inertial effects were negligible [17]. The average pore size of the foams was 0.25 mm in diameter (100 pores per 25.4 mm) as reported by the manufacturer. The foams were cut in cylindrical shapes with radius, a_s, of 27 mm and thickness, H, of 7.6 mm, and then placed in a sample holder filled with castor oil. The foam density was measured using Archimedes' principle as 30 kg/m^3 (consistent with manufacturer specifications). The dynamic viscosity of castor oil is reported as 0.6 Pa · s [18]. The swelling of the dry foam samples was based on prior literature [19,20]. Specifically, prior to swelling, the bottom of the cylindrical foam was fixed to the sample holder using a double-sided tape; samples were then loaded to 70% average normal strain in a nearly unconfined compression setting. Castor oil was then added to the sample holder, and the sample stayed in the castor oil bath in a pre-compressed state for 600 s to avoid trapping air bubbles. Finally, the sample was unloaded slowly and allowed to recover for 600 s. The sample remained fully submerged during the recovery phase. To achieve homogenous and near full-saturation, the load-submerge-unload-recovery process was repeated six times. Repetitions assisted in complete removal of air bubbles trapped in the sample and ensured homogeneity of the foam in the swollen state.

Two flat-ended cylindrical indenters (made of Aluminium 6061-T6), with radii, a, of 4.25 mm and 8.50 mm (Vernier calipers with least count of 0.01 mm) are used to account for length-dependent PVE relaxations and their influence on contact nonlinearities and the damping capacity [11,16].

2.2 Dynamic Mechanical Analysis Setup. In our previous work, we investigated the damping capacity of various indenter–foam dampers via DMA [11]. We used a similar methodology in this study, with broader ranges of strains and strain rates. Previous studies had utilized strains of 1% and average strain rates of 0.04–4 s^{-1}. Here, we extended that range threefold to gauge nonlinear dynamic response of the dampers. In our dynamic tests (Fig. 1(*a*)), the indenter probe was controlled by a universal tester actuator (TA ElectroForce Model 3230; TA Instruments, Eden Prairie, MN). First, a quasistatic pre-compression was applied on the top surface of the foam; then, harmonic oscillations with prescribed amplitudes (displacement-controlled tests) and frequencies were applied. A 10-N load cell attached to the bottom of the sample holder measured the forces throughout the experiments. The expected form of input displacements (primarily single frequency) and measured forces (contains higher harmonics in addition to the primary frequency) can be shown in Fig. 1(*b*).

A quasistatic displacement of $d_0 = 1$ mm was applied on the swollen foams and was held for 600 s for full relaxation to ensure full contact at the beginning of each test. Harmonic excitation amplitude Δd was set to 20, 50, 100, and 200 μm. Therefore, the strain level remained small (~3%) to avoid any material and geometric nonlinearities. The frequency of the harmonic excitations f was set to 1, 3, 10, 20, 50, 70, and 100 Hz in accordance with the earlier studies documenting linear response [11]. Thus, we extend the strain and strain rate level of the harmonic excitation to 0.025 and 10 s^{-1}, respectively. Besides, the peak relaxation frequencies of the 8.5 mm and 4.25 mm indenter–foam dampers were found at around 7.5 Hz and 30 Hz by plotting the phase shift versus frequency (detailed method in Ref. [11]); thus, 1–100 Hz range is suited to study the dampers at their maximal damping capacities. Each measurement reached steady-state after 60 cycles, and the last five cycles of displacement and corresponding force data were reported in the results. The sampling rate was chosen at 5 kHz. Specific damping capacity, defined as $\Psi = W_d/W_s$ where W_d and W_s represent the dissipated and maximum stored energies in a loading cycle [21], was used to quantify the damping capacity of the indenter–foam dampers. The ratio of the higher harmonics to the fundamental harmonic amplitudes in the force response was reported as a measure of nonlinearity.

3 Results and Discussion

3.1 Dynamic Test Results and Damping Capacity. In Fig. 2(*a*), typical steady-state forces are shown and they are measured from 8.5-mm radius indenter–foam damper under harmonic excitations at two extreme cases; almost linear case at $f = 1$ Hz

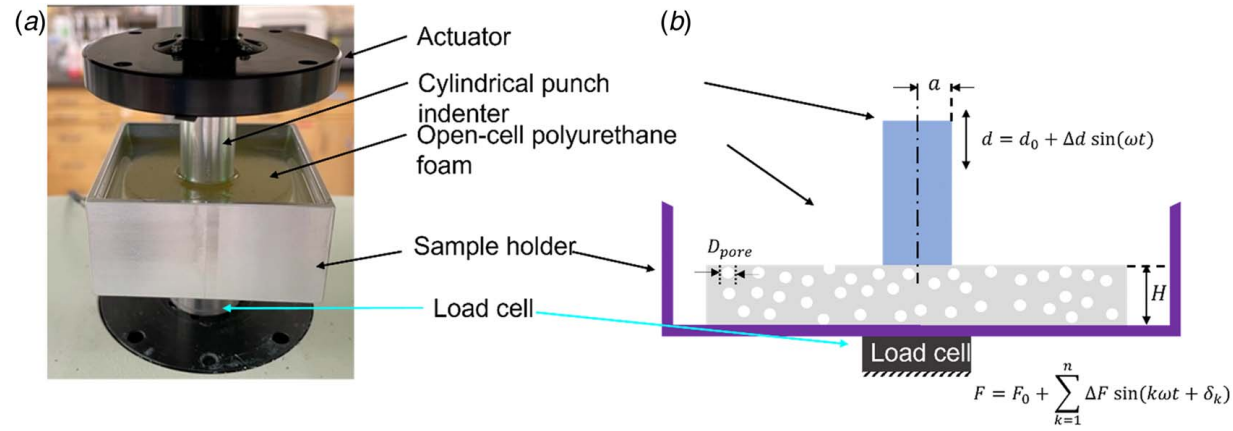

Fig. 1 Experimental setup for dynamic testing of the indenter–foam dampers: (*a*) physical setup and (*b*) schematic with loading and sensing elements. The foams are 54 mm in diameter.

and $\Delta d = 20$ μm, and the most nonlinear case observed at $f =$ 100 Hz and $\Delta d = 200$ μm. Excitations in the form of indenter displacements were purely harmonic for both cases; i.e., negligibly small higher harmonics existed in the signals (blue curves in Fig. 2(*a*)). Forces recorded for the linear case also resembled harmonic signals with amplitudes in the compressive regime (positive magnitudes) throughout the loading cycle, suggesting linear compressive response of the foams. The linearity was also evident from the symmetric force–displacement curve (hysteresis loop) in Fig. 2(*b*) and fundamental harmonic-dominated fast Fourier transform (FFT normalized with respect to the fundamental harmonic peak value) in Fig. 2(*c*). For the nonlinear case, forces exhibited

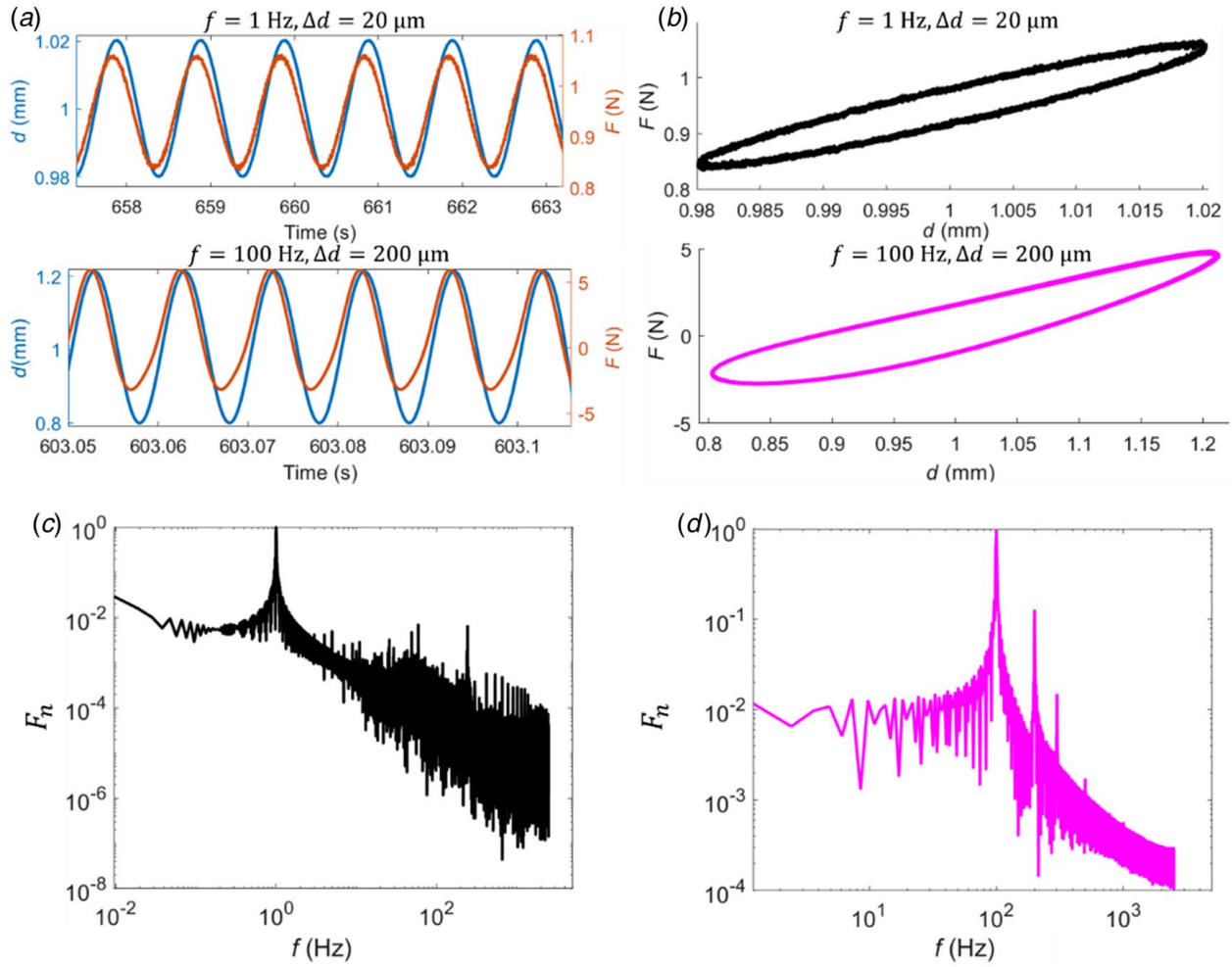

Fig. 2 (*a*) Displacements and forces recorded for 8.5-mm radius indenter–foam damper at $f = 1$ Hz, $\Delta d = 20$ μm (upper subfigure) and $f = 100$ Hz, $\Delta d = 200$ μm (lower subfigure), (*b*) corresponding hysteresis loops, (c) normalized FFT of the force at $f = 1$ Hz, $\Delta d = 20$ μm, and (*d*) normalized FFT of the force at $f = 100$ Hz, $\Delta d = 200$ μm (Color version online.)

partially tensile and partially compressive regimes within a loading cycle and clear asymmetries can be observed in the form of softening in the tension direction (Fig. 2(*a*)). The corresponding hysteresis loop (Fig. 2(*b*)) showed the asymmetry clearly, and FFT of the force (Fig. 2(*d*)) contained higher harmonics at $f_{2,3} = 200$, 300 Hz. Note that the amplitude of the second harmonic was an order of magnitude larger than the third harmonic. Second harmonics were previously shown to dominate the nonlinearities in various other systems with contacts. For instance, partial peeling across rough crack surfaces was the source of contact acoustic nonlinearities in surface wave propagation and corresponding acoustic nonlinearity parameter (defined as the ratio of second to fundamental harmonic amplitudes) yielded a measure of nonlinearity [22]. Further, contact stiffness in shear direction decreases linearly with increasing frictional slip [23–25] and thus delivers quadratic nonlinearity in restoring forces. Borrowing from this literature, we studied the ratio of amplitudes of second and fundamental harmonics (referred to as harmonic ratio in the remainder of the paper) as a function of applied displacement amplitudes and rates in Sec. 3.2.

In the previous studies [9–11], we used phase shift δ between the force and displacements or $\tan(\delta)$ as the measure of damping capacity. However, it only applies to the linear case, and for a nonlinear response, specific damping capacity $\Psi = W_d/W_s$ is more applicable [26]. In this formulation, W_d is the dissipated energy over the full cycle (Eq. (1)) and W_s is the stored energy which is estimated by averaging the maximum stored energies in loading and unloading as in Eq. (2)

$$W_d = \int_{-d_{\min}}^{d_{\max}} (F_l - F_{ul})dx \tag{1}$$

$$W_s = \frac{1}{2}\left(\frac{d_{\max} F_{d_{\max}} + d_{\min} F_{d_{\min}}}{2}\right) \tag{2}$$

Here, F_l and F_{ul} are the forces measured during loading and unloading, respectively. $d_{\max}$ and $d_{\min}$ are the corresponding maximum and minimum displacements. $F_{d_{\max}}$ and $F_{d_{\min}}$ correspond to the values of forces at maximum and minimum displacements [25,26].

To show how the specific damping capacity is influenced by the applied displacement amplitudes and rates, we generated contour plots of specific damping capacity as a function of applied average strains and strain rates in Fig. 3(*a*) for 8.5 mm and Fig. 3(*b*) for 4.25 mm indenter radii. There were 28 data points in total, with four different oscillation amplitudes by seven different loading rates. Linear interpolation was applied to obtain the smooth contour plots. The average applied strain was defined as the indenter displacement divided by the undeformed thickness of the swollen foam, $\Delta d/H$, whereas average strain rate was defined as the displacement loading rate divided by the thickness of the foam, $\dot{d}/H$. At low strain rates, ($\dot{d}/H \ll 1$), the specific damping capacity increased by strain and was almost independent of strain rates. The specific damping capacity reached a maximum value at the lowest strain rate and highest strain. As will be detailed in Secs. 3.2 and 3.3, peeling at the damper interface happened mostly at low strain rates and high strains. The partial loss of contact reduced stored strain energy, and thus, the ratio of dissipation to stored energy defined as maximum damping capacity increased. At intermediate strain rates ($1 < \dot{d}/H < 5$), specific damping capacity followed a diagonal path parallel to the peak relaxation rate of each case (red dashed line in Fig. 3). Those trends suggested that maximum energy capacity was obtained around the peak relaxation rates for both cases when peeling effects are not dominant. This is in line with the linearized analyses and tests reported in our earlier works [9,11]. At higher strain rates ($\dot{d}/H \gg 1$), specific damping capacity decreased from that maximum value gradually since the loading rates were relatively higher than the peak relaxation rates, and so there was less PVE relaxation per loading cycle.

In our previous work, several combinations of indenter radii, polyethylene foams, and swelling agents delivered phase shift δ ranging from 10 deg to 45 deg. This range corresponds to specific damping capacities in the range 1.1–6.3. The specific damping capacities for the indenter-foam damper tested in this paper also reside within this range. Moreover, similar values of the specific damping capacity ($\Psi \sim 0.01$ to 6) were reported for foam materials or elastomers and architected elastic materials in Ref. [27].

3.2 Harmonic Ratio. To show the effect of applied displacement amplitudes and rates on the nonlinearity in the measured force, we plotted in Fig. 4 the ratio of the second to the fundamental harmonic amplitudes as a function of applied average strains and strain rates for cases 8.5 mm (Fig. 4(*a*)) and 4.25 mm (Fig. 4(*b*)) indenter radii. Contour plots for both indenters show a similar trend of harmonic ratio along with the average strain and strain rate. At low strain rates, ($\dot{d}/H \ll 1$), the harmonic ratio increased with strains and was independent of strain rate. The latter trend is expected since damping forces at low strain rates would have negligible contribution compared to elastic forces in the foams and thus would not cause any substantial nonlinearity. The former trend is more difficult to explain. Since strains used in this study were limited to 2.5%, within the typical proportional limit of various open-cell foams [28], neither geometric (higher order strains) nor material nonlinearities could explain the increase in harmonic ratio with strains. An alternative explanation is peeling induced by increasing strains. In this small strain and strain rate regime, the elastic forces grow as strains increase. Increasing elastic forces could overcome adhesive forces holding the indenter and

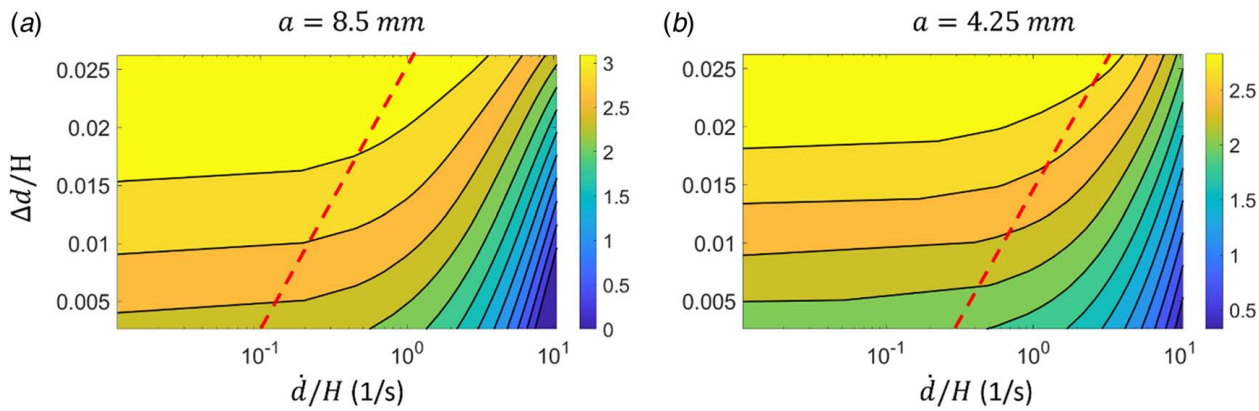

Fig. 3 Contour plots of specific damping capacity Ψ as a function of both average strain and average strain rate for (*a*) the 8.5-mm radius indenter–foam damper and (*b*) the 4.25-mm radius indenter–foam damper (Color version online.)

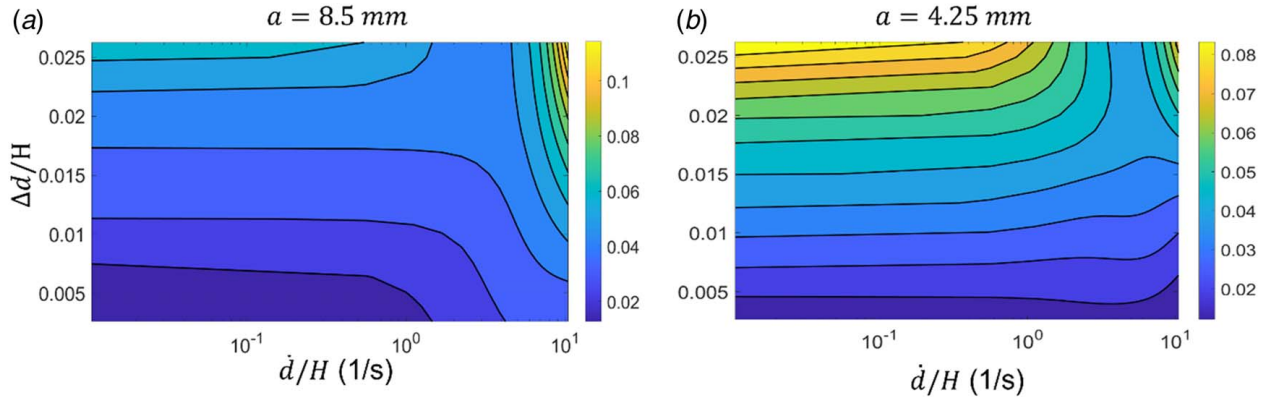

Fig. 4 Contour plots of harmonic ratio as a function of both average strain and average strain rate for (*a*) the 8.5-mm and (*b*) the 4.25-mm radius indenter–foam dampers

foam samples together and compromise full contact condition by partial peeling. Given the stress concentrations, such a peeling would commence at the edge of the flat indenter punches. At higher strain rates ($\dot{d}/H \gg 1$), the harmonic ratio increased with increasing strain and strain rates. If peeling was responsible after the nonlinearity, this trend is also expected since both damping and elastic forces contribute to the total forces built up in the foams, which then could overcome adhesive interactions between indenter and foams.

At high strains ($\Delta d/H \sim 0.025$) and intermediate strain rates ($1 < \dot{d}/H < 5$), the harmonic ratio attained smaller values (local minimum) compared to smaller and higher strain rates at the same high strain level. This trend cannot be explained only by elastic and damping forces built up in the foams overcoming a constant adhesive strength at the indenter–foam interface. Instead, we will resort to rate-dependent adhesion for the possible reason of that local minimum.

3.3 Rate-Dependent Adhesion and Peeling Index. In our previous work [11] and current indenter–foam dampers, adhesion is the only force that kept the interface between the indenter and foams in contact during tension in a vibration cycle. As we discussed in an earlier work [16], the adhesion of PVE materials depends on the degree of relaxation, and hence, it is rate-dependent. This is practically because of how applied mechanical work is distributed within PVE medium to strain, dissipation, bond breakage, and surface creation energies during the peeling process [29–31]. In that respect, experimentally recorded adhesion can only be treated as an apparent property that is coupled to the mechanical response of the material rather than intrinsic adhesive energy of surfaces newly created after peeling. This coupled response can be simply represented by a slider element attached to a lossy material model (standard linear solid) as shown in Fig. 5.

In this model, two springs and a dashpot represent the foam with one dominant relaxation time constant and the slider represent the interface between the indenter and the foam. The constitutive equation relating the force F to the applied displacement d and velocity $\dot{d}$ is shown in Eq. (3)

$$F + \left(\frac{\eta}{k_1 + k_2}\right)\dot{F} - \left(\frac{k_1 k_2}{k_1 + k_2}\right)\left(d + \frac{\eta}{k_2}\dot{d}\right) = 0 \tag{3}$$

where k_1 and k_2 are the stiffness parameters and η is the viscosity. Note that Eq. (3) holds only for complete contact case, i.e., when $F \ll F_p$. F_p is the pull-off force. With increasing force built-up in the foam, peeling commences and progresses until, and when $F = F_p$, the pull-off occurs (i.e., the slider element experiences softening contact stiffness and eventually loses contact). Similar models were used to explain nonlinearities in modal damping [32] and in wave transmission [33] due to interfacial slip. When a harmonic input displacement d is applied to the foam, a resultant periodic force F is transmitted to the slider element, i.e., contact interface. The rate-dependent adhesion force, quantified herein with pull-off forces measured in tack experiments, is denoted as F_p. Accordingly, full separation will occur when the total force in the material exceeds adhesive forces, i.e., $F > F_p$. When $F < F_p$, the interface behavior will range from full to partial contact depending on the magnitude of F relative to F_p. Adopting an ad-hoc approach, we define peeling index as $\mathrm{PI} = F/F_p$. In this definition, $\mathrm{PI} = 1$ means the interface is fully separated and $\mathrm{PI} = 0$ means the interface is under complete contact condition. Note that the forces built up in the foams, F were measured during the dynamic tests discussed earlier. To quantify the peeling index, pull-off forces under different unloading rates are needed.

Adhesion experiments conducted on the same machine and setup shown in Fig. 1 provided pull-off forces. In those experiments, 1-mm static displacement with $0.1\ \mathrm{s}^{-1}$ average strain rate was applied on the foams and was held for 10 min for full relaxation. Then, the indenter was pulled off at different average unloading strain rates ranging from $0.01\ \mathrm{s}^{-1}$ to $10\ \mathrm{s}^{-1}$; i.e., the same range used in the dynamic testing. Forces were recorded at the same sampling rates as in dynamic tests. Each test was repeated twice and showed good repeatability. Typical force–displacement responses obtained from those experiments (positive forces are compressive and negative are tensile per the convention used in the dynamic tests) are shown in Fig. 6. The pull-off force was defined as the maximum negative (tensile) force measured.

Measured pull-off forces normalized to contact areas of indenters (average pull-off stresses) are shown in Fig. 7. Average pull-off stresses increased with unloading rates for both indenters. Similar increases in adhesion with unloading rates were reported for viscoelastic (elastomers in Ref. [34]) and PVE materials (cartilage in Ref. [15]).

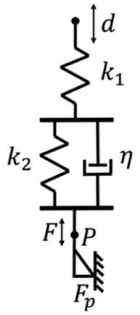

Fig. 5 Representative model of indenter–foam damper with an adhesive interface (modeled as the slider element)

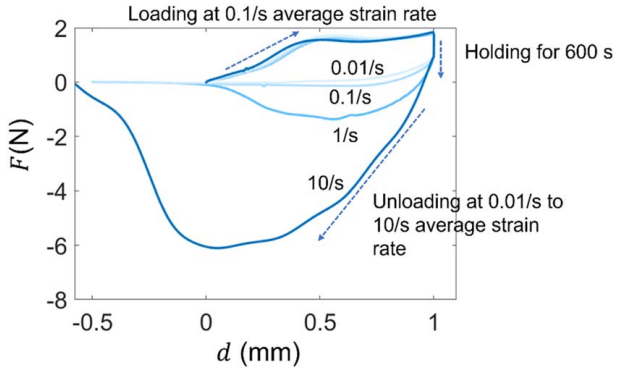

Fig. 6 Raw data of pull-off test for 8.5-mm radius indenter–foam damper under pull-off average strain rates at 0.01/s, 0.1/s, 1/s, and 10/s. Pull-off responses for 4.25-mm radius indenter–foam damper are like the ones shown above.

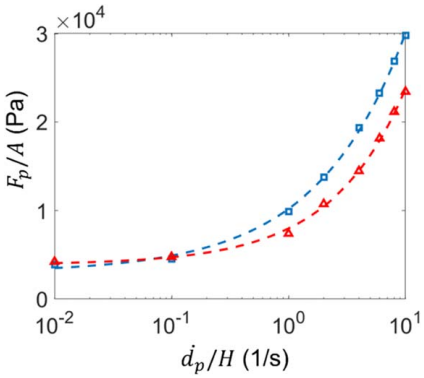

Fig. 7 The average pull-off stress as a function of the average pull-off strain rate for 8.5-mm radius (blue squares) and 4.25-mm radius (red triangles) indenter–foam dampers (Color version online.)

After the adhesion tests, the peeling index was estimated as the ratio of dynamic to pull-off forces measured at corresponding strain rates. The contours of peeling index (PI) values are shown as a function of strain and strain rates in Fig. 8. Similarities between the PI and the harmonic ratio contours are visible in comparing Figs. 8 and 4, respectively. In summary, the degree of nonlinearity observed in measured forces was directly linked to the value of PI.

The trends in PI can be qualitatively explained by the simple model in Fig. 5 and rate-dependent adhesion shown in Fig. 7. At low strain rates, adhesion force F_p remains nearly constant (changes only twofold for 0.01–1 s^{-1} strain rates) while only springs in Fig. 5 contribute to the forces built up in the foam. Hence, the degree of peeling is only a function of strains. This is reflected as horizontal contours of PI in strain rate-strain mapping in Fig. 8. At intermediate to high strain rates, both springs and damper contribute to the forces in the foam but adhesion force increases steeply to suppress peeling partially. That is why the horizontal contours are interrupted and PI attains a local minimum at an intermediate strain. As strain rates further increase, an increase in adhesion forces cannot compensate for the increase in forces in the foam, and so diagonal contours of increasing PI are observed in strain rate-strain mapping. At extremely high loading rates, one would expect damper forces not to contribute to the forces in the foam. In other words, the loading would be too quick for any substantial PVE relaxation, high Peclet number (the ratio of loading to diffusion rate) regime within a loading cycle. In that asymptotic case, we expect the PI contours to exhibit horizontal patterns as in low frequency (nearly quasistatic) asymptote shown in Fig. 8. One key difference in those asymptotes would be that unrelaxed foam is stiffer, and thus, higher PI values would be achieved at higher strain rates compared to the values shown for lower strain rates. Note that extremely high loading rates can be achieved at loading frequencies that are much larger than peak relaxation frequencies of the foam. Our experiments do not cover that asymptote because of the limited frequency bandwidth of the employed universal testing machine.

3.4 Nonlinearity, Peeling, and Reduction in Contact Stiffness. The above discussion relates the nonlinear dynamic response of indenter–foam dampers to the partial peeling at the interface. A similar connection is expected with a reduction in contact stiffness, which scales with the product of Young's modulus and contact length (radius) [35]. Contact stiffness K_{con} can be estimated from the force–displacement curves (Fig. 6). To account for the rate-dependent modulus of the foam and its effect on stiffness, we normalized K_{con} by its initial value at the start of tension K^0_{con} so that $K_n = K_{con}/K^0_{con}$ ranges from 0 to 1 and quantifies the change in contact lengths throughout adhesion tests. Note that similar normalized stiffness measures were used to identify onset of sliding and plastic shearing in the literature [36–38]. The normalized stiffness K_n for both large and small indenters is shown in Fig. 9. As pull-off strain is increased, normalized stiffness decreased because of partial peeling and reduction in contact lengths. For both indenter radii at all but the highest strain rates, normalized stiffness collapsed nearly onto a single curve that smoothly reduces from 1–0.2 as a function of strain. That reduction is less at the highest loading rate. This deviation can be attributed to the complicated peeling dynamics at high adhesion levels measured for 10 s^{-1} cases. As shown in Fig. 6, even after pull-off forces were

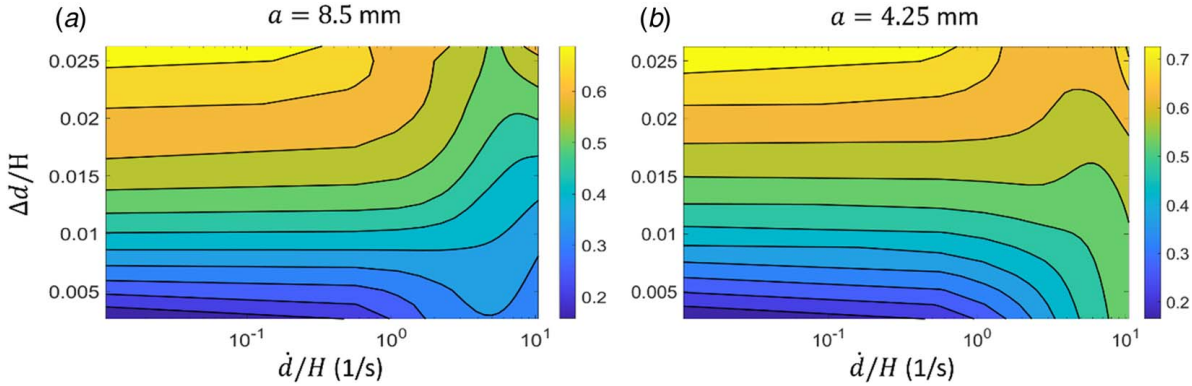

Fig. 8 Contour plots of peeling index (PI) as a function of average strain and average strain rate for (*a*) 8.5-mm radius indenter–foam damper and (*b*) 4.25-mm radius indenter–foam damper

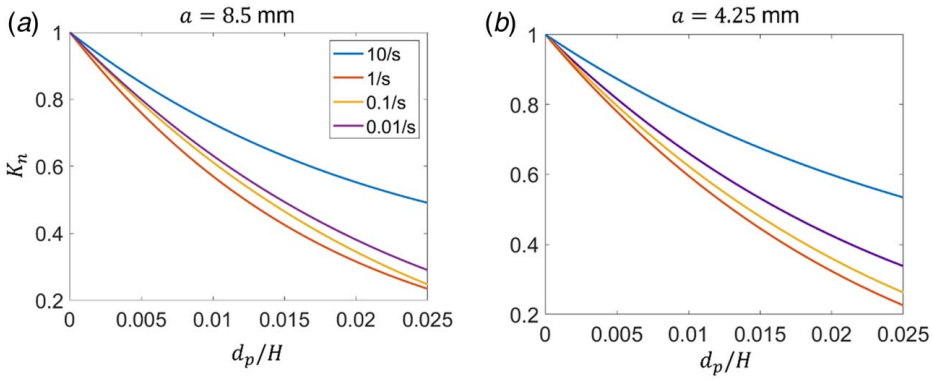

Fig. 9 The normalized stiffness as a function of average strain of (*a*) 8.5-mm radius indenter–foam damper and (*b*) 4.25-mm radius indenter–foam damper

reached, the peeling process continued all the way to negative (tensile) displacements at the highest strain rates. So, larger strain levels are needed to fully separate indenters from the foams at the highest strain rate when compared to the case with the lowest strain rate thanks to the increased adhesion. This helps to explain the local minimum area at high strains ($\Delta d/H \sim 0.025$) and intermediate strain rates ($1 < \dot{d}/H < 5$), as shown in the PI contours in Fig. 8. As strain rates increase within the intermediate strain rates ($1 < \dot{d}/H < 5$), adhesion force increases dramatically as shown in Fig. 7, so adhesion force overcomes the dynamic force applied in the foam and hence the contours appear local minimum. As strain rates further increase, increase in adhesion forces cannot compensate for the increase in forces (both damper and spring forces) in the foam, and so diagonal contours of increasing PI are observed in Fig. 8.

Finally, reduction in normalized stiffness can be linked to the peeling index since both are defined as proportional to contact length. Experimentally evaluated PI and reduction in normalized stiffness ($1 - K_n$) are plotted in Fig. 10 at matched strains for both indenters. As expected, PI and ($1 - K_n$) are linearly related for all but the highest strain rate cases. Complicated transients in the peeling process, as discussed earlier, potentially lead to the breakdown of that linearity at the highest strain rates. Nevertheless, the reduction in contact stiffness, ($1 - K_n$), the decrease in contact lengths, and degree of peeling can be alternatively used to predict the degree of nonlinearity in the dynamic response of the indenter–foam dampers. To do that, one needs a rate-dependent adhesion response of the indenter–foam interface.

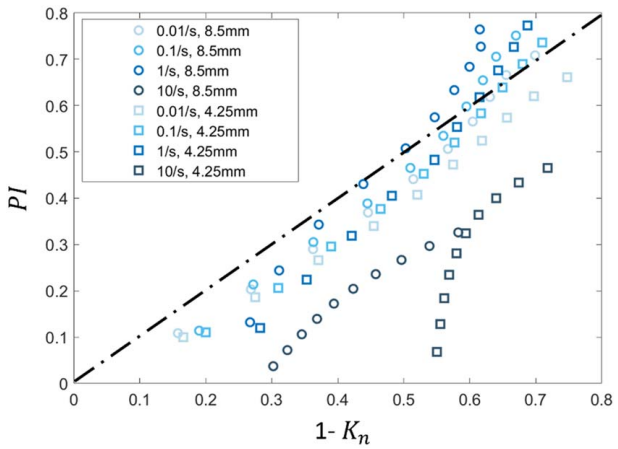

Fig. 10 Scatter plot of PI versus ($1 - K_n$) for both 8.5-mm and 4.25-mm radius indenter–foam damper under average strain rate at 0.01/s, 0.1/s, 1/s, and 10/s

4 Conclusion

In this study, we measured the nonlinear dynamic response of indenter–foam dampers and explained the source of nonlinearity. First, the indenter–foam system has larger damping capacities for larger applied strains. Case with larger applied strain, which has higher damping capacity, showed a significant higher harmonic ratio when compared to the case with lower damping capacity. The higher harmonics in force measurements are observed for strain levels less than 3% on this harmonically excited indenter–foam damper. The presence of higher harmonics is a familiar signature of nonlinear response. Since geometric and constitutive nonlinearities were unlikely due to small strains used in the experiments, we focused on interfacial nonlinearities, specifically adhesion and peeling dynamics, to explain the source of nonlinearities. Then, we analyzed relative magnitudes of second harmonics at various strains and strain rates to obtain nonlinearity maps. We used a simple linear viscoelastic model with a slider element to model adhesive interactions and showed that peeling index and reduction in contact stiffness correlated well with the degree of nonlinear dynamic response. In summary, any of the reduction in contact stiffness, the decrease in contact lengths, and degree of peeling could predict the degree of nonlinearity in the dynamic response of the indenter–foam dampers. The nonlinear dynamic response could complicate the design and limit the usability of indenter–foam dampers. Our findings suggest that increasing adhesion at the indenter–foam interface could suppress those nonlinearities (e.g., via chemical or physical reinforcement of interfaces; see the Appendix for supplemental results on glued indenter–foam interface). However, reinforced interfaces can add local stiffness, reduce permeability, and hence influence force magnitudes and relaxation response of the indenter–foam dampers. Hence, a re-tuning of those reinforced dampers would be needed for the given desired damping criteria.

Interfacial nonlinearities studied here induced second harmonics due to the asymmetric nature of peeling dynamics. Nearly perfect correlation of relative second harmonic amplitudes and peeling index paves the way to vibration-based diagnosis of the adhesive integrity of multi-phasic interfaces (see, for instance, internally resonant testers tuned to nonlinearity order as in Ref. [39]). Since those interfaces are ubiquitous in nature and engineering systems with soft materials, such a diagnosis method could prove useful in various applications.

Acknowledgment

This work is partially supported by the National Science Foundation (Grant Nos. CMMI-1662456 and 1826214) and by the University of Wisconsin-Madison, Office of the Vice Chancellor for Research and Graduate Education with funding from the Wisconsin Alumni Research Foundation. Special thanks to Haocheng Yang,

who carefully proofread the manuscript and provided insightful suggestions.

Conflict of Interest

There are no conflicts of interest.

Data Availability Statement

The data sets generated and supporting the findings of this article are obtainable from the corresponding author upon reasonable request. The authors attest that all data for this study are included in the paper.

Appendix

We repeated the tests with the 8.5-mm indenter glued (Super Unix glue, 2-Methoxyethyl 2-cyanoacrylate, Model: 90015) to the swollen foam at the highest strain and strain rates corresponding to the largest harmonic ratio obtained for the peeling interface (top right corner of Fig. 4(*a*)). The FFT of the measured force is shown in Fig. 11. The FFT was normalized with respect to the magnitude of the first harmonic as in Fig. 2(*d*). The glued interface delivered a 50% lower second harmonic ratio compared to the peeling interface. Note that when hardened, glue-filled zone will add significant local stiffness, reduced permeability, and hence influence force magnitudes and relaxation response. To ensure comparability to the peeling interface cases, a minute amount of glue was applied to the interface in those supplemental tests, and thus, the measured force amplitudes increased only 6.4% compared to the peeling interface case.

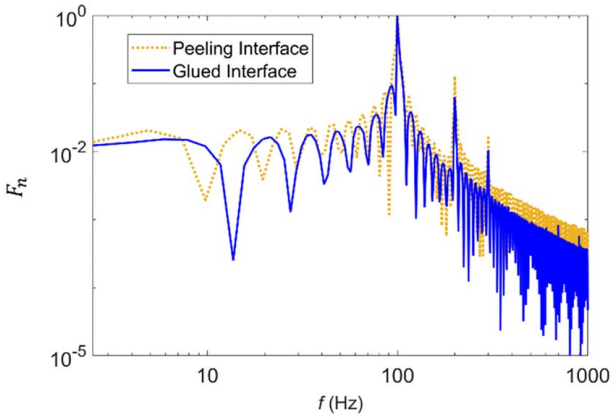

Fig. 11 Comparison of FFT of forces measured at the highest strain and strain rates for glued interface and peeling interface (corresponding to Fig. 4(a) of the paper) cases

References

[1] Soong, T. T., and Spencer Jr, B. F., 2002, "Supplemental Energy Dissipation: State-of-the-Art and State-of-the-Practice," Eng. Struct, **24**(3), pp. 243–259.

[2] Preumont, A., 2018, *Vibration Control of Active Structures: An Introduction*, Springer, Dordrecht, NL.

[3] Soliman, A., and Kaldas, M., 2021, "Semi-Active Suspension Systems From Research to Mass-Market—A Review," J. Low Freq. Noise Vib. Act. Control, **40**(2), pp. 1005–1023.

[4] McNamara, K. P., Love, J. S., Tait, M. J., and Haskett, T. C., 2020, "Response of an Annular Tuned Liquid Damper Equipped With Damping Screens," ASME J. Vib. Acoust., **143**(1), p. 011011.

[5] Wong, W. O., and Wong, C. N., 2020, "Optimal Design of Maxwell-Viscous Coulomb Air Damper With a Modified Fixed Point Theory," ASME J. Vib. Acoust., **143**(3), p. 031002.

[6] Love, J. S., McNamara, K. P., Tait, M. J., and Haskett, T. C., 2019, "Series-Type Pendulum Tuned Mass Damper-Tuned Sloshing Damper," ASME J. Vib. Acoust., **142**(1), p. 011003.

[7] Javidialesaadi, A., and Wierschem, N. E., 2018, "Three-Element Vibration Absorber–Inerter for Passive Control of Single-Degree-of-Freedom Structures," ASME J. Vib. Acoust., **140**(6), p. 061007.

[8] Verbaan, C. A., Peters, G. W., and Steinbuch, M., 2017, "The Advantage of Linear Viscoelastic Material Behavior in Passive Damper Design-With Application in Broad-Banded Resonance Dampers for Industrial High-Precision Motion Stages," J. Sound Vib., **386**, pp. 242–250.

[9] Liu, L., Usta, A. D., and Eriten, M., 2017, "A Broadband Damper Design Inspired by Cartilage-Like Relaxation Mechanisms," J. Sound Vib., **406**, pp. 1–14.

[10] Boz, U., and Eriten, M., 2018, "A Numerical Investigation of Damping in Fuzzy Oscillators With Poroelastic Coating Attached to a Host Structure," J. Sound Vib., **417**, pp. 277–293.

[11] Han, G., Boz, U., Liu, L., Henak, C. R., and Eriten, M., 2020, "Indenter–Foam Dampers Inspired by Cartilage: Dynamic Mechanical Analyses and Design," ASME J. Vib. Acoust., **142**(5), p. 051113.

[12] Gent, A. N., and Schultz, J., 1972, "Effect of Wetting Liquids on the Strength of Adhesion of Viscoelastic Material," J. Adhes., **3**(4), pp. 281–294.

[13] Maugis, D., and Barquins, M., 1980, "Fracture Mechanics and Adherence of Viscoelastic Solids," *Adhesion and Adsorption of Polymers*, L-H Lee, ed., Springer US, Boston, MA, pp. 203–277.

[14] Lorenz, B., Krick, B. A., Mulakaluri, N., Smolyakova, M., Dieluweit, S., Sawyer, W. G., and Persson, B. N. J., 2013, "Adhesion: Role of Bulk Viscoelasticity and Surface Roughness," J. Phys.: Condens. Matter, **25**(22), p. 225004.

[15] Han, G., and Eriten, M., "Effect of Relaxation-Dependent Adhesion on Pre-sliding Response of Cartilage," R. Soc. Open Sci., **5**(5), p. 172051.

[16] Han, G., Eriten, M., and Henak, C. R., 2020, "Rate-Dependent Adhesion of Cartilage and Its Relation to Relaxation Mechanisms," J. Mech. Behav. Biomed. Mater., **102**, p. 103493.

[17] Comiti, J., Sabiri, N., and Montillet, A., 2000, "Experimental Characterization of Flow Regimes in Various Porous Media—III: Limit of Darcy's or Creeping Flow Regime for Newtonian and Purely Viscous Non-Newtonian Fluids," Chem. Eng. Sci., **55**(15), pp. 3057–3061.

[18] Quinchia, L., Delgado, M., Valencia, C., Franco, J., and Gallegos, C., 2010, "Viscosity Modification of Different Vegetable Oils With EVA Copolymer for Lubricant Applications," Ind. Crops Prod., **32**(3), pp. 607–612.

[19] Nia, H. T., Bozchalooi, I. S., Li, Y., Han, L., Hung, H.-H., Frank, E., Youcef-Toumi, K., Ortiz, C., and Grodzinsky, A., 2013, "High-Bandwidth AFM-Based Rheology Reveals That Cartilage Is Most Sensitive to High Loading Rates at Early Stages of Impairment," Biophys. J., **104**(7), pp. 1529–1537.

[20] Nia, H. T., Han, L., Li, Y., Ortiz, C., and Grodzinsky, A., 2011, "Poroelasticity of Cartilage at the Nanoscale," Biophys. J., **101**(9), pp. 2304–2313.

[21] Martz, E. O., Lakes, R. S., and Park, J. B., 1996, "Hysteresis Behaviour and Specific Damping Capacity of Negative Poisson's Ratio Foams," Cell. Polym., **15**(5), pp. 349–364.

[22] Oberhardt, T., Kim, J.-Y., Qu, J., and Jacobs, L. J., 2016, "A Contact Mechanics Based Model for Partially-Closed Randomly Distributed Surface Microcracks and Their Effect on Acoustic Nonlinearity in Rayleigh Surface Waves," AIP Conference Proceedings, Minneapolis, MN, July 26–31, 2015, p. 020024.

[23] Eriten, M., Polycarpou, A. A., and Bergman, L. A., 2011, "Physics-Based Modeling for Fretting Behavior of Nominally Flat Rough Surfaces," Int. J. Solids Struct., **48**(10), pp. 1436–1450.

[24] Eriten, M., Chen, S., Usta, A. D., and Yerrapragada, K., 2020, "In Situ Investigation of Load-Dependent Nonlinearities in Tangential Stiffness and Damping of Spherical Contacts," ASME J. Tribol., **143**(6), p. 061501.

[25] Parel, K. S., Paynter, R. J., and Nowell, D., 2020, "Linear Relationship of Normal and Tangential Contact Stiffness With Load," Proc. R. Soc. A, **476**(2243), p. 20200329.

[26] Lakes, R., and Lakes, R. S., 2009, *Viscoelastic Materials*, Cambridge University Press, New York.

[27] Haghpanah, B., Shirazi, A., Salari-Sharif, L., Guell Izard, A., and Valdevit, L., 2017, "Elastic Architected Materials With Extreme Damping Capacity," Extreme Mech. Lett., **17**, pp. 56–61.

[28] Gibson, L. J., Ashby, M. F., and Harley, B. A., 2010, *Cellular Materials in Nature and Medicine*, Cambridge University Press, Cambridge, UK.

[29] Yang, T., Yang, X., Huang, R., and Liechti, K. M., 2019, "Rate-Dependent Traction-Separation Relations for a Silicon/Epoxy Interface Informed by Experiments and Bond Rupture Kinetics," J. Mech. Phys. Solids, **131**, pp. 1–19.

[30] Léger, L., and Creton, C., 2008, "Adhesion Mechanisms at Soft Polymer Interfaces," Philos. Trans. R. Soc., A, **366**(1869), pp. 1425–1442.

[31] Barthel, E., and Frétigny, C., 2009, "Adhesive Contact of Elastomers: Effective Adhesion Energy and Creep Function," J. Phys. D: Appl. Phys., **42**(19), p. 195302.

[32] Segalman, D. J., Allen, M. S., Eriten, M., and Hoppman, K., 2016, "Experimental Assessment of Joint-Like Modal Models for Structures," International Design Engineering Technical Conferences and Computers and Information in Engineering Conference, Boston, MA, Aug. 2–5, 2015, American Society of Mechanical Engineers Digital Collection, p. V008T13A025.

[33] Moore, K. J., Kurt, M., Eriten, M., Dodson, J. C., Foley, J. R., Wolfson, J. C., McFarland, D. M., Bergman, L. A., and Vakakis, A. F., 2017, "Nonlinear

Parameter Identification of a Mechanical Interface Based on Primary Wave Scattering," Exp. Mech., **57**(9), pp. 1495–1508.
[34] Violano, G., and Afferrante, L., 2019, "Adhesion of Compliant Spheres: An Experimental Investigation," Procedia Struct. Integrity, **24**, pp. 251–258.
[35] Johnson, K. L., 1985, *Contact Mechanics*, Cambridge University Press, Cambridge, UK.
[36] Brizmer, V., Kligerman, Y., and Etsion, I., 2007, "A Model for Junction Growth of a Spherical Contact Under Full Stick Condition," ASME J. Tribol., **129**(4), pp. 783–790.
[37] Patil, D. B., and Eriten, M., 2015, "Frictional Energy Dissipation in Spherical Contacts Under Presliding: Effect of Elastic Mismatch, Plasticity and Phase Difference in Loading," ASME J. Appl. Mech., **82**(1), p. 011005.
[38] Patil, D. B., and Eriten, M., 2014, "Effects of Interfacial Strength and Roughness on the Static Friction Coefficient," Tribol. Lett., **56**(2), pp. 355–374.
[39] Kurt, M., Slavkin, I., Eriten, M., McFarland, D. M., Gendelman, O. V., Bergman, L. A., and Vakakis, A. F., 2014, "Effect of 1:3 Resonance on the Steady-State Dynamics of a Forced Strongly Nonlinear Oscillator With a Linear Light Attachment," Arch. Appl. Mech., **84**(8), pp. 1189–1203.